JACS
JOURNAL OF THE AMERICAN CHEMICAL SOCIETY

Subscriber access provided by ISTANBUL TEKNIK UNIV

Article

GdY*Tt* (*Tt* = Si or Ge): Effect of Metal Substitution on Structure, Bonding, and Magnetism

Sumohan Misra, and Gordon J. Miller

J. Am. Chem. Soc., **2008**, 130 (42), 13900-13911 • DOI: 10.1021/ja802848r • Publication Date (Web): 26 September 2008

Downloaded from http://pubs.acs.org on February 8, 2009

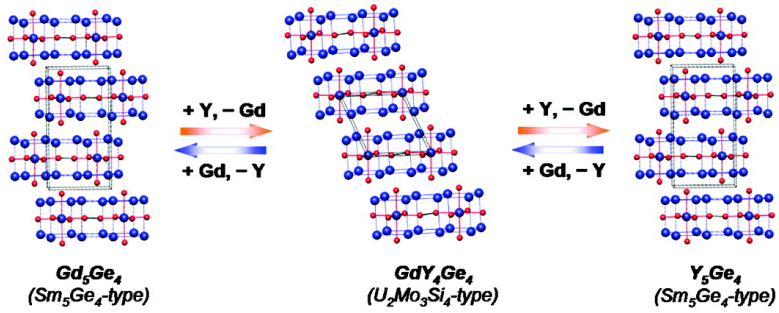

More About This Article

Additional resources and features associated with this article are available within the HTML version:

- Supporting Information
- Access to high resolution figures
- Links to articles and content related to this article
- Copyright permission to reproduce figures and/or text from this article

View the Full Text HTML

ACS Publications
High quality. High impact.

Journal of the American Chemical Society is published by the American Chemical Society. 1155 Sixteenth Street N.W., Washington, DC 20036

J|A|C|S
ARTICLES

Published on Web 09/26/2008

$Gd_{5-x}Y_xTt_4$ (Tt = Si or Ge): Effect of Metal Substitution on Structure, Bonding, and Magnetism

Sumohan Misra and Gordon J. Miller*

Department of Chemistry and Ames Laboratory, Iowa State University, Ames, Iowa 50011

Received April 22, 2008; E-mail: gmiller@iastate.edu

Abstract: A crystallographic study and theoretical assessment of the Gd/Y site preferences in the $Gd_{5-x}Y_xTt_4$ (Tt = Si, Ge) series prepared by high-temperature methods is presented. All structures for the $Gd_{5-x}Y_xSi_4$ system belong to the orthorhombic, Gd_5Si_4-type (space group *Pnma*). For the $Gd_{5-x}Y_xGe_4$ system, phases with $x < 3.6$ and $x \geq 4.4$ adopt the orthorhombic, Sm_5Ge_4-type structure. For the composition range of $3.6 \leq x \leq 4.2$, a monoclinic, $U_2Mo_3Si_4$-type structure (space group $P2_1/c$) occurs as the majority phase. This structure type has not been previously observed in the RE_5T_4 (T = Si, Ge, Ga) system and differs from the known monoclinic structure of $Gd_5Si_2Ge_2$-type (space group $P2_1/a$) because all Ge···Ge contacts between slabs are equivalent. The structural relationships between the Sm_5Ge_4-type and the $U_2Mo_3Si_4$-type structures are discussed. Single crystal refinements of the occupancies for the three sites for Gd/Y atoms in the asymmetric unit reveal a partially ordered arrangement of Gd and Y atoms. TB-LMTO-ASA calculations were performed to study these atomic distributions as well as to elucidate possible electronic forces that might drive the structural variation. These results illustrate the importance of one of the Gd/Y-sites in shaping the magnetic and structural features observed in $Gd_{5-x}Y_xTt_4$ system. The magnetic properties of some of the $Gd_{5-x}Y_xTt_4$ phases are also reported. Germanides with $x \leq 2$ show a metamagnetic-type transition similar to Gd_5Ge_4 from 57−92(2) K. As the Y concentration increases ($3 \leq x \leq 4$), these phases exhibit at least ferrimagnetic ordering with transition temperatures ranging from 15−31(2) K to the paramagnetic state.

Introduction

The $RE_5(Si_xGe_{1-x})_4$ (RE = rare-earth element) family of compounds is characterized by an intimate relationship between chemical composition, crystal structure, and magnetism.[1−8] There is an intriguing interplay between several different, yet closely related, crystal structures, all of which are based on characteristic slabs and the nature of their spontaneous magnetic ordering. During the past decade, the discovery of a giant magnetocaloric effect (MCE) in $Gd_5Si_2Ge_2$, along with other extraordinary magnetic properties, such as a colossal magnetostriction and giant magnetoresistance,[9−16] has encouraged the rare-earth-tetrelide systems at the 5:4 stoichiometry to be subjects of broad interest, especially $Gd_5(Si_xGe_{1-x})_4$.

Most of the research activity to date has emphasized the chemistry, physics, and materials science of Gd_5T_4 systems where T = Si, Ge, Ga, Sn, or their various combinations.[17−23] For $Gd_5(Si_xGe_{1-x})_4$, as the Si/Ge ratio varies, it shows two amazing changes for their room temperature structures (Figure 1). All structures involve stackings of $[Gd_5T_4]$ slabs. At low Si concentrations ($x \leq 0.30$), the orthorhombic Sm_5Ge_4-type

(1) Pecharsky, V. K.; Gschneidner, K. A., Jr. *Phys. Rev. B* **1997**, *78*, 4494.
(2) Pecharsky, V. K.; Gschneidner, K. A., Jr. *Appl. Phys. Lett.* **1997**, *70*, 3299.
(3) Pecharsky, V. K.; Gschneidner, K. A., Jr. *J. Magn. Magn. Mater.* **1997**, *167*, L179.
(4) Miller, G. J. *Chem. Soc. Rev.* **2006**, *35*, 799.
(5) Giguere, A.; Foldeaki, M.; Ravi Gopal, R.; Bose, T. K.; Frydman, A. *Phys. Rev. Lett.* **1999**, *83*, 2262.
(6) Gschneidner, K. A., Jr.; Pecharsky, V. K.; Duijin, H. G. M.; Levin, E. M. *Phys. Rev. Lett.* **2000**, *85*, 4190.
(7) Pecharsky, A. O., Jr.; Gschneidner, K. A., Jr.; Pecharsky, V. K. *J. Appl. Phys.* **2003**, *93*, 4722.
(8) Gschneidner, K. A., Jr.; Pecharsky, V. K.; Tsokol, A. O. *Rep. Prog. Phys.* **2005**, *68*, 1479.
(9) Morellon, L.; Blasco, J.; Algarabel, P. A.; Ibara, M. R. *Phys. Rev. B* **2000**, *62*, 1022.
(10) Morellon, L.; Algarabel, P. A.; Ibara, M. R.; Blasco, J.; Garcia-Landa, B. *Phys. Rev. B* **1998**, *58*, R14721.
(11) Magen, C.; Morellon, L.; Algarabel, P. A.; Marquina, C.; Ibara, M. R. *J. Phys.: Condens. Matter* **2003**, *15*, 2389.
(12) Morellon, L.; Stankiewicz, J.; Garcia-Landa, B.; Algarabel, P. A.; Ibara, M. R. *Appl. Phys. Lett.* **1998**, *73*, 3462.
(13) Levin, E. M.; Pecharsky, V. K.; Gschneidner, K. A., Jr. *Phys. Rev. B* **1999**, *60*, 7993.
(14) Levin, E. M.; Pecharsky, V. K.; Gschneidner, K. A., Jr. *J. Magn. Magn. Mater.* **2000**, *210*, 181.
(15) Levin, E. M.; Pecharsky, V. K.; Gschneidner, K. A., Jr. *Phys. Rev. B* **2001**, *63*, 174110.
(16) Stankiewicz, J.; Morellon, L.; Algarabel, P. A.; Ibara, M. R. *Phys. Rev. B* **2000**, *61*, 12651.
(17) Choe, W.; Pecharsky, V. K.; Pecharsky, A. O.; Gschneidner, K. A., Jr.; Young, V. G., Jr.; Miller, G. J. *Phys. Rev. Lett.* **2000**, *84*, 4617.
(18) Choe, W.; Miller, G. J.; Meyers, J.; Chumbley, S.; Pecharsky, A. O. *Chem. Mater.* **2003**, *15*, 1413.
(19) Smith, G. S.; Johnson, Q.; Tharp, A. G. *Acta Crystallogr.* **1967**, *22*, 269.
(20) Pecharsky, A. O., Jr.; Pecharsky, V. K.; Schindler, C. E. *J. Alloys Compd.* **2002**, *338*, 126.
(21) Choe, W.; Pecharsky, A. O.; Wörle, M.; Miller, G. J. *Inorg. Chem.* **2003**, *42*, 8223.
(22) Mozharivskyj, Y.; Choe, W.; Pecharsky, A. O.; Miller, G. J. *J. Am. Chem. Soc.* **2003**, *125*, 15183.
(23) Mozharivskyj, Y.; Tsokol, A. O.; Miller, G. J. *Z. Kristallogr.* **2006**, *221*, 493.

10.1021/ja802848r CCC: $40.75 **© 2008 American Chemical Society**

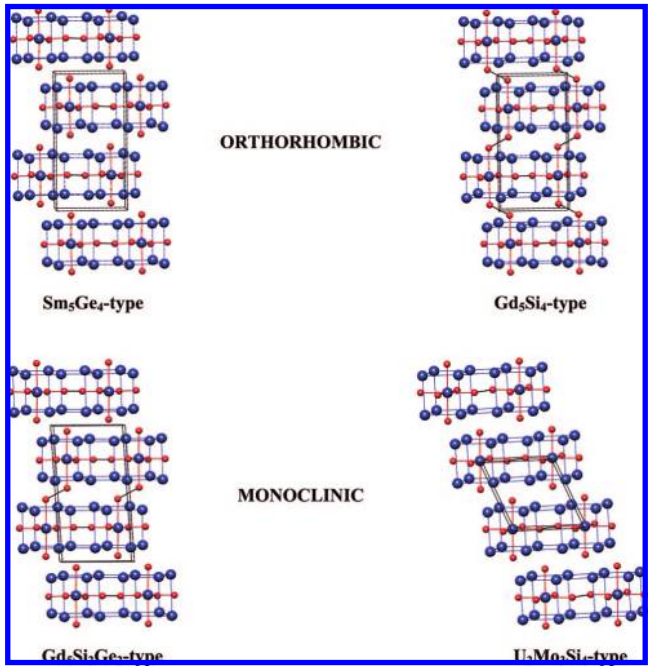

Figure 1. Projections of four crystal structures observed for various RE_5T_4 (T = Si, Ge, Ga) systems. Blue atoms represent RE metal and red atoms represent T atoms.

structure exists, which is characterized by the absence of any interslab Si(Ge)−Si(Ge) bonds; at high Si concentrations ($x \geq 0.56$), the orthorhombic Gd_5Si_4-type structure occurs and features the presence of interslab Si(Ge)−Si(Ge) covalent bonds. At intermediate Si compositions ($0.40 \leq x \leq 0.503$), the monoclinic $Gd_5Si_2Ge_2$-type structure exists, which displays only one-half of the Si(Ge)−Si(Ge) pairs, short enough for covalent bonding. The structural transition in this series is due to a correlation between the distribution of Si and Ge at the *Tt*-sites between the slabs (Si has a preference for the intraslab sites and Ge prefers the interslab positions) and the nature of the *Tt*···*Tt* interslab contacts.[24] The dependence of the crystal structure on valence electron counts have also been investigated, as in the $Gd_5Ga_xGe_{4-x}$ system,[22] where a decrease in valence electron concentration through substitution of three-valent, size equivalent Ga for four-valent Ge results in lower population of antibonding $T-T$ (interslab) states with subsequent shortening and formation of $T-T$ interslab dimers, thereby leading to a structural transition.

The physical and chemical properties of tetrelides for other rare-earth or mixtures of rare-earth elements at the 5:4 stoichiometry have been explored to a much lesser extent, especially when RE = Y, La or Lu.[25,26] We report here the results obtained for a systematic investigation of the effect of replacing Gd with Y on the structural features and magnetic properties in both pseudobinary Si and Ge systems. Not only is Y smaller than Gd,[27] but Y has no f electrons, although both Gd and Y are isoelectronic in their valance shell configurations. Hence, Y will dilute the magnetic moments associated with Gd and should affect magnetic ordering patterns as well as ordering temperatures. Such behavior also exists in the binary Gd−Y alloys.[28] Gd and Y both adopt the *hcp* crystal structure type and form a continuous series of solid solutions.[28] These alloys show ferromagnetic behavior for Gd content exceeding 60 atomic % but antiferromagnetic ordering below 60 atomic %; Y itself is Pauli paramagnetic. Furthermore, the Curie temperatures for the ferromagnetic phases increase from about 95(2)−281(1) K as Gd content increases above 60 atomic %.[28] The Néel temperatures for alloys with Gd content less than 60% were in the range of about 111(2)−197(2) K.[28] Therefore, dilution of Gd with Y changes the magnetic properties continuously, but then undergoes a significant change in long-range order at a specific composition.

In the Gd−Y−Ge system, there are variations in the magnetic ordering as well as a transformation from the orthorhombic Sm_5Ge_4-type[29] to a new monoclinic $U_2Mo_3Si_4$-type[30] (Figure 1) structure for certain compositions. This structure is different from the known monoclinic structure of $Gd_5Si_2Ge_2$-type and has not been reported before in the RE_5T_4 system. Thus, this structure becomes the eighth structure type established for the RE_5T_4 system.[4,22]

Experimental Section

Syntheses. Samples of $Gd_{5-x}Y_xSi_4$, where $x = 0$, 1, 2, 3, and 4, and $Gd_{5-x}Y_xGe_4$, where $x = 0$, 1, 2, 3, 3.2, 3.4, 3.6, 3.8, 4, 4.2, 4.4, 4.6, 4.8, and 5.0 were prepared by arc-melting its constituent elements in an argon atmosphere on a water-cooled copper hearth. The starting materials were pieces of gadolinium (99.99 wt %, Materials Preparation Center, Ames Laboratory), yttrium (99.99 wt %, Materials Preparation Center, Ames Laboratory), silicon (99.9999 wt %, Alfa Aesar), and germanium (99.9999 wt %, Alfa Aesar). Each ingot had a total weight of about 1 g and was remelted six times to ensure homogeneity. Weight losses during melting were less than 0.1 wt %. To check for possible phase transformation and the distribution of rare-earth atoms among the metal sites upon annealing, the samples were heated in evacuated silica tubes, at a rate of 4 °C/min to 800 °C, and were then annealed for 1 week. In the end, the tubes were quenched in ice water.

Powder X-ray Diffraction. The as-cast samples were examined by powder X-ray diffraction for identification and to assess phase purity. Powder patterns were obtained using an Enraf-Nonius Guinier camera using monochromatized Cu Kα radiation (λ = 1.54187 Å). To probe the purity and homogeneity of all phases, all diffraction patterns were analyzed by full-profile Rietveld refinement using *LHPM RIETICA* software.[31] Only the scale factor and the lattice parameters of each phase were refined. The isotropic displacement parameters of all atoms in each phase were assumed to be the same. For $Gd_{5-x}Y_xSi_4$, the profile residuals, R_p, varied from about 1.89−4.24 and derived Bragg residuals, R_B, varied from about 1.56−6.58. For $Gd_{5-x}Y_xGe_4$, the profile residuals, R_p, varied from about 2.33−4.73 (for pure phases) and from about 2.36−9.68 (for mixed phases). Their derived Bragg residuals, R_B, varied from about 2.29−5.15 (for pure phases) and from about 2.45−15.90 (for mixed phases). Figure 2 shows a schematic plot of the diffraction patterns for the four different phases existing in the RE_5T_4 system, patterns that were used for phase identification. There is a significant difference among these plots in the 2θ range 22−32°, which, therefore, acts as a fingerprinting region to identify the different phases.

(24) Misra, S.; Miller, G. J. *J. Solid State Chem.* **2006**, *179*, 2290.
(25) Elbicki, J. M.; Zhang, L. Y.; Obermyer, R. T.; Wallace, W. E. *J. Appl. Phys.* **1991**, *69*, 5571.
(26) Mudryk, Y.; Paudayl, D.; Pecharsky, V. K.; Gschneidner, K. A., Jr.; Misra, S.; Miller, G. J., in preparation.
(27) Shannon, R. D. *Acta Crystallogr., Sect. A: Found. Crystallogr.* **1976**, *32*, 751.
(28) Thoburn, W. C.; Legvold, S.; Spedding, F. H. *Phys. Rev.* **1958**, *110*, 1298.
(29) Holtzberg, F.; Gambino, R. J.; McGuire, T. R. *J. Phys. Chem. Solids* **1967**, *28*, 2283.
(30) Richter, K. W.; Franzen, H. F. *J. Solid State Chem.* **2000**, *150*, 347.
(31) Hunter, B. A. *International Union of Crystallography Commission on Powder Diffraction Newsletter* **1998**, *20*, 21.

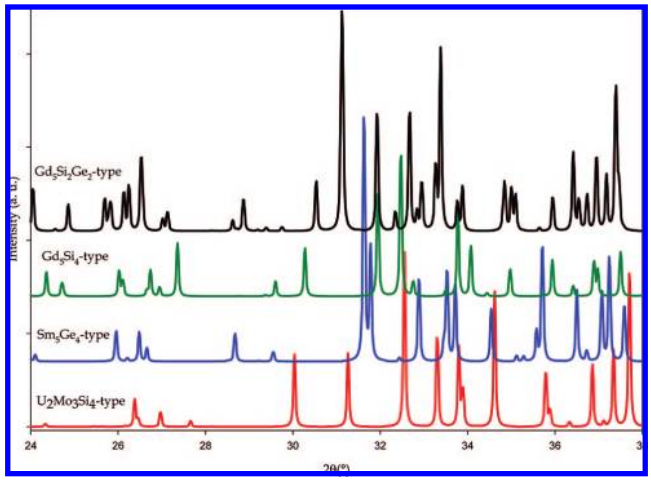

Figure 2. Schematic representation of powder X-ray diffraction patterns of four different types of structure types existing in the RE_5T_4 system.

Single-Crystal X-ray Crystallography. Several single crystals from the as-cast samples were mounted on the tips of glass fibers. Room temperature intensity data were collected on a Bruker Smart Apex CCD diffractometer with Mo Kα radiation ($\lambda = 0.71073$ Å) and a detector-to-crystal distance of 5.990 cm. Data were collected over a full sphere of reciprocal space by taking three sets of 606 frames with 0.3° scans in ω with an exposure time of 10 s per frame. The 2θ range extended from 4° to 57°. The *SMART*[32] software was used for data acquisition. Intensities were extracted and then corrected for Lorentz and polarization effects by the *SAINT*[32] program. Empirical absorption corrections were accomplished with *SADABS*,[32] which is based on modeling a transmission surface by spherical harmonics employing equivalent reflections with $I > 3\sigma(I)$. Structure solutions and refinements were performed with the *SHELXTL*[32] package of crystallographic programs.

Magnetic Property Measurements. Magnetic measurements were carried out using a Lake Shore ac/dc susceptometer-magnetometer, model 7225 on polycrystalline samples weighing about 0.25 g. These included dc magnetic susceptibility measurements between about 4 and 300 K and isothermal magnetization measurements in dc magnetic fields varying from 0 to 50 kOe. For the susceptibility measurements, the samples were first cooled under zero magnetic field (zfc) and then the measurements were carried out on heating under a 10 kOe magnetic field. The measurements were then repeated upon cooling with the magnetic field turned on (fc). All data were corrected for T-independent contributions.

Electronic Structure Calculations. Tight-binding, linear muffin-tin orbital (TB-LMTO) electronic band structure calculations with the atomic spheres approximation (ASA) were carried out using the Stuttgart program[33] on various models of Gd_5Ge_4, Gd_4YGe_4 GdY_4Ge_4, and Y_5Ge_4. Exchange and correlation were treated in a local spin density approximation. All relativistic effects except spin-orbit coupling were taken into account using a scalar relativistic approximation. The radii of the Wigner-Seitz (WS) spheres were obtained by requiring the overlapping potential to be the best possible approximation to the full potential according to an automatic procedure, no empty spheres were necessary.[34] The WS radii determined by this procedure are in the ranges 1.791−2.001 Å for Gd, 1.799−2.090 Å for Y, and 1.516−1.686 Å for Ge. The basis set included Gd 6*s*, 6*p*, and 5*d* orbitals, Y 5*s*, 5*p*, and 4*d* orbitals, and Ge 4*s*, 4*p*, and 4*d* orbitals. The Gd 4*f* orbitals were treated as core wave functions occupied by seven valence electrons. Furthermore, the Ge 4*d* orbitals were treated by the Löwdin downfolding technique.[33] The **k**-space integrations to determine total energies and densities of states were evaluated by the tetrahedron method using 75−136 **k**-points (orthorhombic) and 170−512 **k**-points (monoclinic) in the irreducible wedges of the first Brillouin zones.

Results and Discussion

Structural Features. The powder X-ray diffraction patterns for all $Gd_{5-x}Y_xSi_4$ samples ($0.0 \le x \le 4.0$) could be completely indexed by the orthorhombic (space group *Pnma*), Gd_5Si_4-type structure. The lattice parameters obtained from powder X-ray diffraction are presented in Table 1. The crystallographic data, atomic coordinates, site occupancies, and isotropic displacement parameters obtained from single crystal X-ray diffraction are listed in the Supporting Information. Previously, Elbicki and

Table 1. Lattice Parameters for $Gd_{5-x}Y_xSi_4$ As Obtained by Powder X-ray Diffraction[a]

x	*a* (Å)	*b* (Å)	*c* (Å)	*V*′[b] (Å^3)
0	7.4880(6)	14.750(1)	7.7476(6)	213.9(1)
1	7.4634(4)	14.7123(9)	7.7421(4)	212.53(8)
2	7.4411(4)	14.6754(9)	7.7301(4)	211.03(8)
3	7.4245(4)	14.6419(8)	7.7170(4)	209.73(8)
4	7.4105(4)	14.6087(8)	7.7062(4)	208.56(8)

[a] Gd_5Si_4-type, space group *Pnma* (No. 62), Cu Kα radiation, 2θ range = 10−100°, $T = 298(2)$ K, $Z = 4$. [b] V' = unit cell volume per formula unit.

Table 2. Lattice Parameters for $Gd_{5-x}Y_xGe_4$ As Obtained by Powder X-ray Diffraction[a]

x	structure type(s)	*a* (Å)	*b* (Å)	*c* (Å)	*β* (°)	*V*′[b] (Å^3)
0	Sm_5Ge_4	7.6984(4)	14.8372(8)	7.7872(4)		222.4(1)
1	Sm_5Ge_4	7.6842(4)	14.8070(8)	7.7690(4)		221.0(1)
2	Sm_5Ge_4	7.6675(4)	14.7795(8)	7.7504(4)		219.6(1)
3	Sm_5Ge_4[c] + *$U_2Mo_3Si_4$*	7.6559(9)	14.7553(18)	7.7346(10)		218.4(2)
		present in trace amounts				
3.2	Sm_5Ge_4[c] + *$U_2Mo_3Si_4$*	7.6519(6)	14.7476(11)	7.7319(6)		218.1(1)
		present in trace amounts				
3.4	Sm_5Ge_4[c] + *$U_2Mo_3Si_4$*	7.6441(3) *8.097(7)*	14.7354(6) *7.723(6)*	7.7210(3) *7.690(6)*	*113.32(5)*	217.4(0) *220.8(6)*
3.6	*Sm_5Ge_4* + $U_2Mo_3Si_4$[c]	*7.646(1)* 8.0277(31)	*14.738(2)* 7.7401(28)	*7.718(1)* 7.6501(28)	113.08(3)	*217.4(2)* 218.6(3)
3.8	*Sm_5Ge_4* + $U_2Mo_3Si_4$[c]	*7.644(1)* 7.9971(22)	*14.738(2)* 7.7562(24)	*7.712(1)* 7.6235(20)	113.09(2)	*217.2(2)* 217.5(2)
4	*Sm_5Ge_4* + $U_2Mo_3Si_4$[c]	*7.735(1)* 8.0067(9)	*14.759(1)* 7.7540(10)	*7.679(1)* 7.6174(8)	113.04(1)	*219.15(3)* 217.6(1)
4.2	*Sm_5Ge_4* + $U_2Mo_3Si_4$[c]	*7.720(3)* 8.0022(5)	*14.717(5)* 7.7460(5)	*7.676(3)* 7.6061(5)	113.00(1)	*218.0(6)* 217.0(0)
4.4	Sm_5Ge_4[c] + *$U_2Mo_3Si_4$*	7.6389(8) *8.031(2)*	14.7196(15) *7.730(3)*	7.7103(9) *7.619(2)*	*113.14(2)*	216.7(2) *217.5(3)*
4.6	Sm_5Ge_4	7.6373(5)	14.7097(10)	7.7037(5)		216.4(1)
4.8	Sm_5Ge_4	7.6335(5)	14.6985(9)	7.6982(5)		215.9(1)
5	Sm_5Ge_4	7.6316(2)	14.6976(3)	7.6966(2)		215.8(0)

[a] Lattice parameters for the minority phases are shown in italics. Space group for Sm_5Ge_4-type ($Z = 4$) and $U_2Mo_3Si_4$-type ($Z = 2$) structures are *Pnma* (No. 62) and $P2_1/c$ (No. 14), respectively, Cu Kα radiation, 2θ range = 10−100°, $T = 298(2)$ K. [b] V' = unit cell volume per formula unit. [c] Majority phase as determined from Rietveld refinement.

(32) *XRD Single Crystal Software*; Bruker Analytical X-ray Systems: Madison, WI, 2002.
(33) (a) Andersen, O. K. *Phys. Rev. B* **1975**, *12*, 3060. (b) Andersen, O. K.; Jepsen, O. *Phys. Rev. Lett.* **1984**, *53*, 2571. (c) Andersen, O. K.; Jepsen, O.; GÏotzel, D. In *Highlights of Condensed-Matter Theory*; Bassani, F., Fumi, F., Tosi, M. P., Eds.; North-Holland: New York, 1985. (d) Andersen, O. K. *Phys. Rev. B* **1986**, *34*, 2439. (e) Tank, R. W.; Jepsen, O.; Burckhardt, A.; Andersen, O. K. *TB-LMTO-ASA program*, Version 4.7c; Max-Planck-Institut für Festkörperforschung: Stuttgart, Germany, 1994.
(34) Jepsen, O.; Andersen, O. K. *Z. Phys. B* **1995**, *97*, 35.

Table 3. Crystallographic Data for $Gd_{5-x}Y_xGe_4$ (x = 0, 1, 2, 3, 3.2, and 3.4) As Obtained by Single Crystal X-ray Diffraction[a]

x	0	1	2	3	3.2	3.4
loaded composition	Gd_5Ge_4	Gd_4YGe_4	$Gd_3Y_2Ge_4$	$Gd_2Y_3Ge_4$	$Gd_{1.8}Y_{3.2}Ge_4$	$Gd_{1.6}Y_{3.4}Ge_4$
refined composition	Gd_5Ge_4	$Gd_{4.02(6)}Y_{0.98}Ge_4$	$Gd_{2.96(5)}Y_{2.04}Ge_4$	$Gd_{1.91(4)}Y_{3.09}Ge_4$	$Gd_{1.74(5)}Y_{3.26}Ge_4$	$Gd_{1.55(6)}Y_{3.45}Ge_4$
independent reflections	1098	1081	1083	1068	1072	1061
No. of parameters	47	50	50	50	50	50
final R indices [$I > 2\sigma(I)$]	$R1 = 0.0385$, $wR2 = 0.0831$	$R1 = 0.0461$, $wR2 = 0.0864$	$R1 = 0.0485$, $wR2 = 0.0881$	$R1 = 0.0503$, $wR2 = 0.0799$	$R1 = 0.0493$, $wR2 = 0.0895$	$R1 = 0.0628$, $wR2 = 0.1179$
peak/hole (e/Å^3)	3.085/−1.817	2.570/−2.138	2.332/−2.332	2.183/−2.326	2.743/−2.284	3.593/−2.331

[a] Space group *Pnma* (No. 62), Mo Kα radiation, 2θ range = 4−57°, T = 298(2) K, Z = 4.

Table 4. Crystallographic Data for $Gd_{5-x}Y_xGe_4$ (x = 3.6, 4.4, 4.6, 4.8, and 5.0) As Obtained by Single Crystal X-ray Diffraction[a]

x	3.6	4.4	4.6	4.8	5.0
loaded composition	$Gd_{1.4}Y_{3.6}Ge_4$	$Gd_{0.6}Y_{4.4}Ge_4$	$Gd_{0.4}Y_{4.6}Ge_4$	$Gd_{0.2}Y_{4.8}Ge_4$	Y_5Ge_4
refined composition	$Gd_{1.26(4)}Y_{3.74}Ge_4$	$Gd_{0.61(5)}Y_{4.39}Ge_4$	$Gd_{0.29(3)}Y_{4.71}Ge_4$	$Gd_{0.17(3)}Y_{4.83}Ge_4$	Y_5Ge_4
independent reflections	1076	1078	1091	1069	1070
No. of parameters	50	50	50	50	47
final R indices [$I > 2\sigma(I)$]	$R1 = 0.0524$, $wR2 = 0.0914$	$R1 = 0.0611$, $wR2 = 0.1109$	$R1 = 0.0437$, $wR2 = 0.0758$	$R1 = 0.0423$, $wR2 = 0.0838$	$R1 = 0.0482$, $wR2 = 0.0798$
peak/hole (e/Å^3)	2.225/−1.902	3.442/−2.025	1.841/−1.626	3.196/−1.489	1.730/−1.642

[a] Space group *Pnma* (No. 62), Mo K_α radiation, 2θ range = 4−57°, T = 298(2) K, Z = 4.

co-workers[25] had reported powder X-ray diffraction results on these phases for $0.0 \le x \le 2.0$. In our investigation with both powder and single crystal X-ray diffraction for $0.0 \le x \le 4.0$, we obtain similar results. Moreover, we also observe that Gd and Y are nonrandomly distributed over the three RE metal sites: there is preferential occupation of Y at the M3 site (center of the pseudocube), whereas Gd prefers the M1 sites. As expected, due to the smaller size of Y compared to Gd,[27] the unit-cell volume gradually decreases with increasing concentration of Y.

For the $Gd_{5-x}Y_xGe_4$ system, three distinct composition ranges exist as identified by powder X-ray diffraction. For $x < 3.6$ and $x \ge 4.4$, the orthorhombic, Sm_5Ge_4-type structure forms as the majority phase, and for the composition range of $3.6 \le x \le 4.2$, the monoclinic $U_2Mo_3Si_4$-type structure is observed as the majority phase. The lattice parameters obtained from Rietveld refinement of the powder data are presented in Table 2. The crystallographic data, atomic coordinates, site occupancies, and isotropic displacement parameters from single crystal X-ray diffraction are shown in Tables 3−7. To check for possible phase transformation upon annealing, the sample with $x = 4.0$, having the monoclinic $U_2Mo_3Si_4$-type structure was annealed at 800 °C for 1 week and then a powder diffraction pattern was measured. The diffraction pattern was similar to the pattern before annealing with no additional peaks.

The orthorhombic crystal structure has six atoms in the asymmetric unit: three crystallographically independent sites for Gd or Y metal atoms and three distinct sites for the tetrelide atoms. All three rare-earth metal sites (in both structures) exhibit mixed site occupancies, with Gd (or the larger rare-earth atom) having a preference for the M1 site and Y (or the smaller rare-earth atom) having a preference for the M3 site (see Figure 3) as observed in Gd−Y−Si, Gd−La−Ge,[26] Gd−Lu−Ge,[26] and Gd−Sc−Ge[35] systems. In comparison to the orthorhombic structure, the asymmetric unit of the monoclinic structure has five atoms: three distinct sites for Gd or Y metal atoms and just two distinct sites for the tetrelide atoms. This monoclinic structure has never been previously reported in RE_5T_4 systems. However, it has been observed in various ternary compounds with lanthanide and actinide elements, for example, in

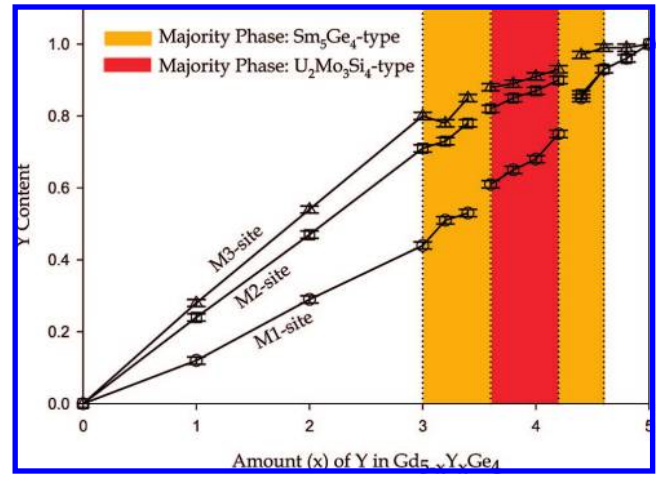

Figure 3. Y occupation in each M site of $Gd_{5-x}Y_xGe_4$ as a function of Y concentration, x, as obtained from single crystal X-ray diffraction. The shaded regions delineate the two-phase regions as observed from powder X-ray diffraction.

$RE_2Mo_3Si_4$ where RE = Dy, Er, Ho, Tb, Tm, Y,[36] and also in $U_2M_3Tt_4$, where M = V, Mo, and W and Tt = Si and Ge.[37] Nevertheless, the monoclinic $U_2Mo_3Si_4$ structure-type shows remarkable similarities with the Sm_5Ge_4-type structure. Both crystal structures are built from nearly identical 3^2434 nets of Gd/Y atoms. Two such nets are placed over one another to form two-dimensional slabs with additional Gd/Y atoms in pseudocubic coordination (M3 site) and Ge2, Ge3 (in case of orthorhombic structure), and Ge2 atoms (in case of monoclinic structure) in trigonal prismatic voids. These crystal structures differ from one other in the manner in which these neighboring slabs stack with respect to each other. In the orthorhombic structure, each slab has reflection symmetry through the M3, T2, and T3 sites, and the first and the second slabs are shifted but related by inversion symmetry. This results in the slabs being arranged in a way that the interslab Ge1···Ge1 contacts form a herringbone pattern along the *b*-direction. In the monoclinic

(35) Misra, S.; Miller, G. J., to be published.

(36) Bodak, O. I.; Gorelenko, Y. K.; Yarovets, V. I.; Skolozdra, R. V. *Inorg. Mater.* **1984**, *20*, 741.

(37) Bihan, T. L.; Nöel, H. *J. Alloys Compd.* **1995**, *227*, 44.

Table 5. Atomic Coordinates, Site Occupancies, and Isotropic Displacement Parameters for $Gd_{5-x}Y_xGe_4$ ($x \leq 3.6$; $x \geq 4.4$) As Obtained by Single Crystal X-ray Diffraction[a]

atom		*x*	*y*	*z*	occupancy[b]	U_{eq}, (Å^2)[c]	atom		*x*	*y*	*z*	occupancy[b]	U_{eq}, (Å^2)[c]
			Gd_5Ge_4							$Gd_{1.26(4)}Y_{3.74}Ge_4$			
M1	8d	0.9758(1)	0.4000(1)	0.1782(1)	1	0.009(1	M1	8d	0.9730(1)	0.4001(1)	0.1772(1)	0.39(1)	0.011(1)
M2	8d	0.6233(1)	0.3832(1)	0.8387(1)	1	0.008(1)	M2	8d	0.6227(1)	0.3829(1)	0.8392(1)	0.18(1)	0.009(1)
M3	4c	0.2097(1)	3/4	0.4992(1)	1	0.008(1)	M3	4c	0.2122(2)	3/4	0.4992(2)	0.12(1)	0.008(1)
Ge1	8d	0.7821(2)	0.4560(1)	0.5332(2)	1	0.009(1)	Ge1	8d	0.7815(2)	0.4558(1)	0.5326(2)	1	0.010(1)
Ge2	4c	0.0817(2)	3/4	0.1127(2)	1	0.010(1)	Ge2	4c	0.0819(3)	3/4	0.1155(2)	1	0.010(1)
Ge3	4c	0.3261(2)	3/4	0.8657(2)	1	0.009(1)	Ge3	4c	0.3315(2)	3/4	0.8638(2)	1	0.011(1)
			$Gd_{4.02(6)}Y_{0.98}Ge_4$							$Gd_{0.61(5)}Y_{4.39}Ge_4$			
M1	8d	0.9755(1)	0.4001(1)	0.1781(1)	0.88(1)	0.010(1)	M1	8d	0.9702(2)	0.3992(1)	0.1758(2)	0.15(1)	0.013(1)
M2	8d	0.6235(1)	0.3831(1)	0.8387(1)	0.76(1)	0.009(1)	M2	8d	0.6205(2)	0.3835(1)	0.8389(2)	0.14(1)	0.011(1)
M3	4c	0.2101(2)	3/4	0.4988(2)	0.72(1)	0.009(1)	M3	4c	0.2141(3)	3/4	0.4989(3)	0.03(1)	0.009(1)
Ge1	8d	0.7822(2)	0.4562(1)	0.5336(2)	1	0.010(1)	Ge1	8d	0.7801(2)	0.4555(1)	0.5304(2)	1	0.013(1)
Ge2	4c	0.0819(3)	3/4	0.1135(3)	1	0.010(1)	Ge2	4c	0.0840(3)	3/4	0.1168(3)	1	0.011(1)
Ge3	4c	0.3273(3)	3/4	0.8653(3)	1	0.010(1)	Ge3	4c	0.3338(3)	3/4	0.8642(3)	1	0.011(1)
			$Gd_{2.96(5)}Y_{2.04}Ge_4$							$Gd_{0.29(3)}Y_{4.71}Ge_4$			
M1	8d	0.9749(1)	0.4002(1)	0.1779(1)	0.71(1)	0.010(1)	M1	8d	0.9700(1)	0.3995(1)	0.1760(1)	0.07(1)	0.010(1)
M2	8d	0.6234(1)	0.3831(1)	0.8388(1)	0.53(1)	0.009(1)	M2	8d	0.6205(1)	0.3831(1)	0.8394(1)	0.07(1)	0.009(1)
M3	4c	0.2105(2)	3/4	0.4990(2)	0.46(1)	0.009(1)	M3	4c	0.2143(2)	3/4	0.4989(2)	0.01(1)	0.008(1)
Ge1	8d	0.7825(2)	0.4560(1)	0.5335(2)	1	0.010(1)	Ge1	8d	0.7796(1)	0.4556(1)	0.5311(1)	1	0.010(1)
Ge2	4c	0.0816(3)	3/4	0.1144(3)	1	0.010(1)	Ge2	4c	0.0839(2)	3/4	0.1164(2)	1	0.010(1)
Ge3	4c	0.3284(3)	3/4	0.8647(3)	1	0.010(1)	Ge3	4c	0.3350(2)	3/4	0.8635(2)	1	0.010(1)
			$Gd_{1.91(4)}Y_{3.09}Ge_4$							$Gd_{0.17(3)}Y_{4.83}Ge_4$			
M1	8d	0.9744(1)	0.4002(1)	0.1777(1)	0.56(1)	0.010(1)	M1	8d	0.9696(1)	0.3992(1)	0.1759(1)	0.04(1)	0.011(1)
M2	8d	0.6233(1)	0.3829(1)	0.8391(1)	0.29(1)	0.008(1)	M2	8d	0.6205(1)	0.3832(1)	0.8392(1)	0.04(1)	0.009(1)
M3	4c	0.2116(2)	3/4	0.4990(2)	0.20(1)	0.008(1)	M3	4c	0.2143(1)	3/4	0.4988(2)	0.01(1)	0.009(1)
Ge1	8d	0.7823(2)	0.4559(1)	0.5331(2)	1	0.009(1)	Ge1	8d	0.7798(1)	0.4556(1)	0.5310(1)	1	0.011(1)
Ge2	4c	0.0811(2)	3/4	0.1155(2)	1	0.009(1)	Ge2	4c	0.0840(2)	3/4	0.1167(2)	1	0.010(1)
Ge3	4c	0.3299(2)	3/4	0.8639(2)	1	0.010(1)	Ge3	4c	0.3352(2)	3/4	0.8633(2)	1	0.009(1)
			$Gd_{1.74(5)}Y_{3.26}Ge_4$							Y_5Ge_4			
M1	8d	0.9737(1)	0.4001(1)	0.1772(1)	0.49(1)	0.011(1)	M1	8d	0.9692(1)	0.3993(1)	0.1758(1)	1	0.010(1)
M2	8d	0.6228(1)	0.3830(1)	0.8390(1)	0.27(1)	0.009(1)	M2	8d	0.6204(1)	0.3829(1)	0.8396(1)	1	0.008(1)
M3	4c	0.2118(2)	3/4	0.4992(2)	0.22(1)	0.009(1)	M3	4c	0.2145(2)	3/4	0.4988(2)	1	0.008(1)
Ge1	8d	0.7817(2)	0.4558(1)	0.5331(2)	1	0.010(1)	Ge1	8d	0.7797(1)	0.4556(1)	0.5314(1)	1	0.009(1)
Ge2	4c	0.0818(3)	3/4	0.1155(3)	1	0.009(1)	Ge2	4c	0.0840(2)	3/4	0.1163(2)	1	0.009(1)
Ge3	4c	0.3309(3)	3/4	0.8642(3)	1	0.010(1)	Ge3	4c	0.3353(2)	3/4	0.8635(2)	1	0.009(1)
			$Gd_{1.55(6)}Y_{3.45}Ge_4$										
M1	8d	0.9737(2)	0.4002(1)	0.1773(2)	0.47(1)	0.014(1)							
M2	8d	0.6229(2)	0.3830(1)	0.8391(2)	0.22(1)	0.011(1)							
M3	4c	0.2119(3)	3/4	0.4990(3)	0.15(1)	0.010(1)							
Ge1	8d	0.7815(3)	0.4559(1)	0.5333(3)	1	0.013(1)							
Ge2	4c	0.0814(3)	3/4	0.1159(3)	1	0.012(1)							
Ge3	4c	0.3306(3)	3/4	0.8637(3)	1	0.013(1)							

[a] Coordinates are represented in accordance with similar previously reported structure types. [b] All M1, M2, and M3 sites are fully occupied with a mixture of Gd and Y atoms. Only Gd occupations are listed. The only exception is Gd_5Ge_4 and Y_5Ge_4, where the M1, M2, and M3 sites are fully occupied by Gd and Y atoms, respectively. [c] U(eq) is defined as one-third of the trace of the orthogonalized U_{ij} tensor.

$U_2Mo_3Si_4$-type structure, each slab has inversion symmetry at the M3 sites, and adjacent layers are related by translational symmetry, resulting in a stacking pattern that creates inversion symmetry between slabs along the stacking direction. Due to these different symmetry characteristics, the arrangements of the M1 and M2 metal positions are different in the two structures, although every cube surrounding the M3 positions contains 4 M1 and 4 M2 sites. In the orthorhombic structure, the two faces of the cube perpendicular to the *c*-direction are either all M1 or all M2. On the other hand, for the monoclinic structure, the two faces of the cube perpendicular to the *b*-direction are 50% M1 and 50% M2 in an alternating pattern, which preserves the inversion center at the M3 site.

The other monoclinic structure observed in the RE_5T_4 system, the $Gd_5Si_2Ge_2$-type, adopts the space group $P2_1/a$, which is a proper subgroup of *Pnma*, and contains nine atoms in the asymmetric unit with the M1 and M2 sites each splitting into two pairs (M1a, M1b and M2a, M2b) and the *T*1 site also splitting into a pair of distinct sites (*T*1a, *T*1b). Hence, when compared with the monoclinic $U_2Mo_3Si_4$-type structure, the $Gd_5Si_2Ge_2$-type forms two sets of inequivalent interslab (*T*1−*T*1) contacts, resulting in one-half of these pairs short enough for covalent bonding. The stacking pattern of the slabs remains similar to the Sm_5Ge_4-type structure.

Variations of selected interatomic distances across the $Gd_{5-x}Y_xGe_4$ series ($3.0 \leq x \leq 5.0$) near the crystal structure changes are illustrated in Figure 4. The structural figures display the various contacts, matching the color code of the plots. The vertical dotted lines delineate the region where the monoclinic phase is observed. For all plots there are distinct deviations when $x = 3.8-4.2$, marking the region for the structural transition. The largest variations occur for certain intraslab M···M and M···Ge distances, and arise because the change in symmetry (orthorhombic to monoclinic) creates equidistant bond lengths. These are marked as black open triangles and inverted triangles in the plots and as dashed bonds in the figures. The graphs, moreover, identify certain pervasive features of the entire series: (a) Ge−Ge contacts between adjacent slabs are nonbonding,

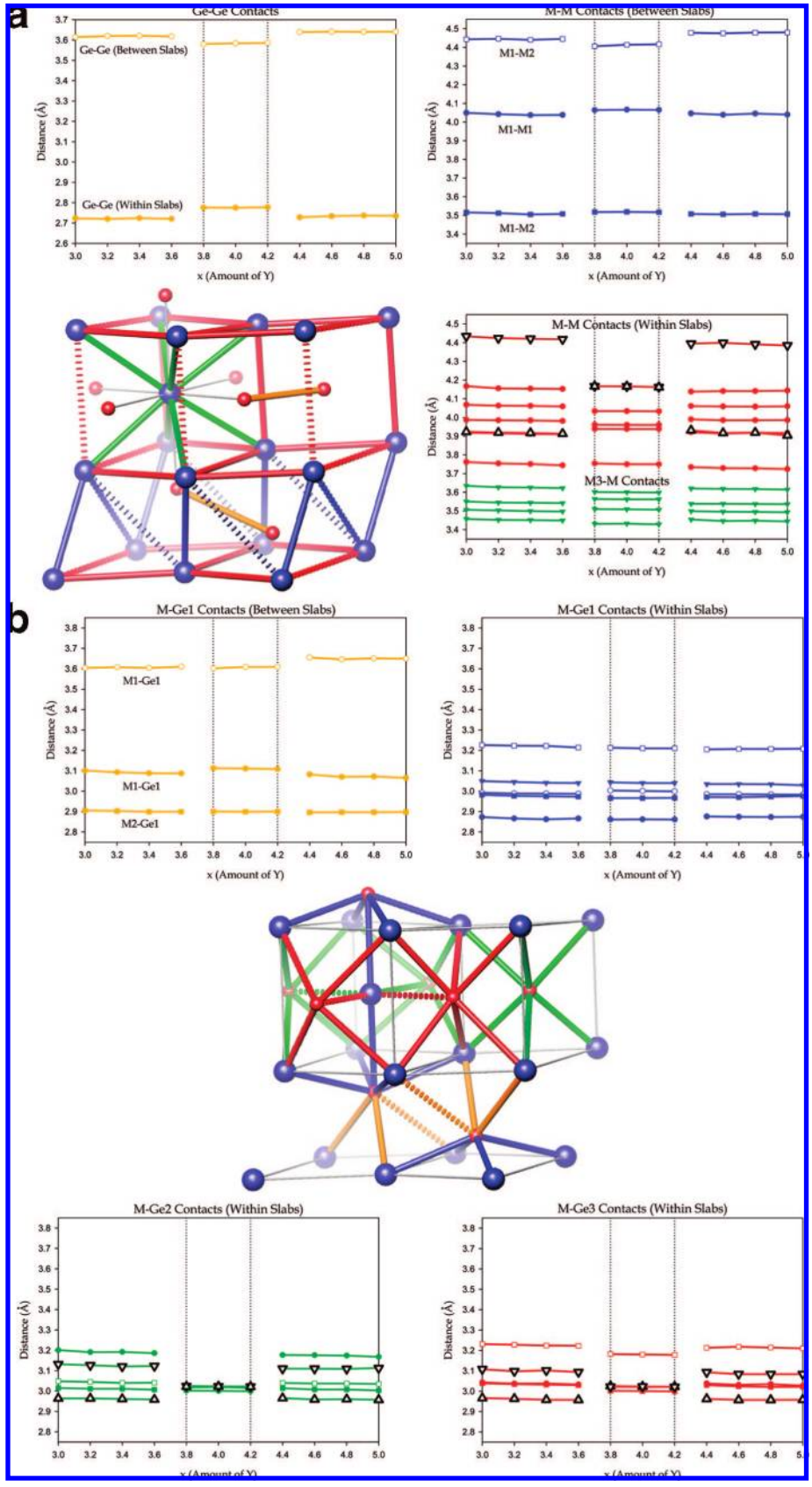

Figure 4. (a) Interatomic distance variations in $Gd_{5-x}Y_xGe_4$ as a function of Y concentration, x. These graphs illustrate trends in Ge−Ge and M−M distances. The distance scales on all M−M graphs are identical to illustrate the relative magnitudes. (b) Interatomic distance variations in $Gd_{5-x}Y_xGe_4$ as a function of Y concentration, x. These graphs illustrate trends in M−Ge distances. The distance scales on all graphs are identical to illustrate the relative magnitudes. The structural figures show the various interatomic distances presented by the graphs in their respective colors. Blue spheres are metal (Gd/Y), and red spheres are Ge sites.

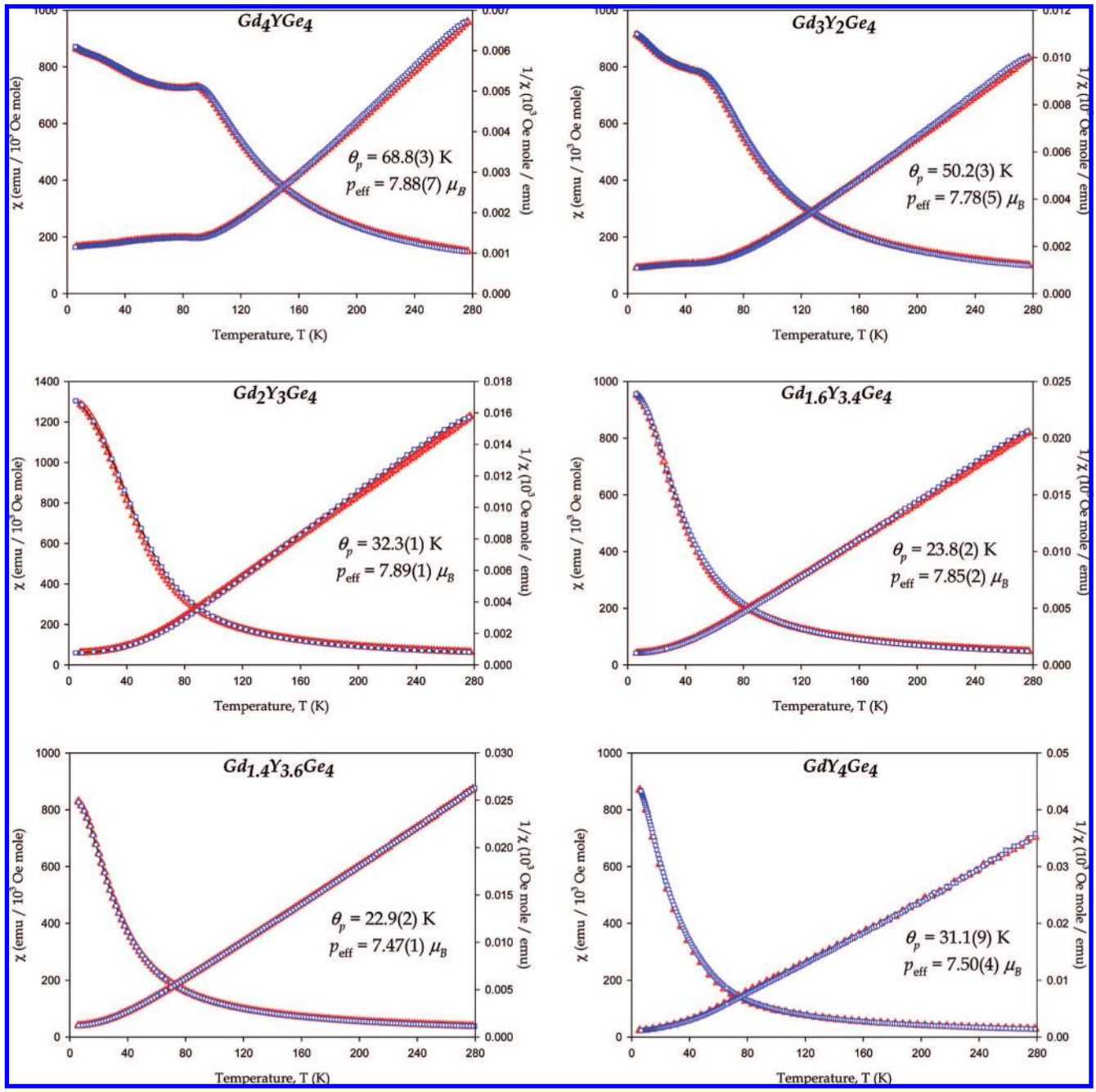

Figure 5. Magnetic susceptibility plots for $Gd_{5-x}Y_xGe_4$ series. Red triangles are data for the heating cycles (zfc) and blue circles are data for the cooling cycles (fc) with $H = 10$ kOe.

or, at most, weakly bonding; (b) M1−Ge and M2−Ge contacts between adjacent slabs are more significant (solid orange bonds in Figure 4b) for holding the slabs together than the Ge−Ge contacts; (c) there is a single M−M (M1−M2) interaction between slabs (solid blue bonds in Figure 4a) that occurs at each M1 or M2 site and exhibits a very short distance (ca. 3.50 Å); and (d) the most significant M−M interactions within each slab involve the M3 sites. We will discuss some of the impacts of these geometrical features in more detail in the subsequent section on electronic structure.

Magnetism. Figure 5 illustrates the magnetic susceptibility measurements in a 10 kOe field for the $Gd_{5-x}Y_xGe_4$ series. The Gd-rich phases ($x = 1$ and 2) show a metamagnetic-type transition at 92 and 57 K, respectively, similar to Gd_5Ge_4, which shows this transition at 128 K (T_N). The reduction in transition temperature can be explained by dilution of the magnetic Gd sites by Y in this system.[28] The curves also show a Curie−Weiss behavior above these transitions. The Y-rich phases ($x = 3-4$), in contrast, undergo ferrimagnetic-type ordering showing Curie−Weiss behavior at high temperatures. The $M(H)$ plots for the above phases are available in Supporting Information, which also reiterates the presence of metamagnetic and ferrimagnetic-type behavior as none of the phases show saturation in fields up to 50 kOe. The paramagnetic Curie temperatures, θ_p, decrease with increasing Y concentration, but increases for $x = 4$. The Curie temperatures, T_C, were estimated for the ferrimagnetic phases ($x = 3.0$, 3.4, 3.6, and 4.0) from dM/dT versus T plots to be 31(2), 24(2), 20(2), and 15(2) K,

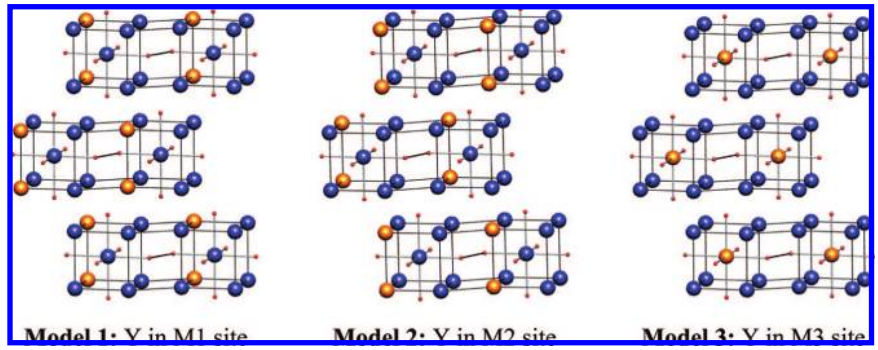

Figure 6. Three model structures of Gd_4YGe_4 studied by TB-LMTO-ASA and LSDA calculations. Blue spheres are Gd, orange spheres are Y, and smaller red spheres are Ge.

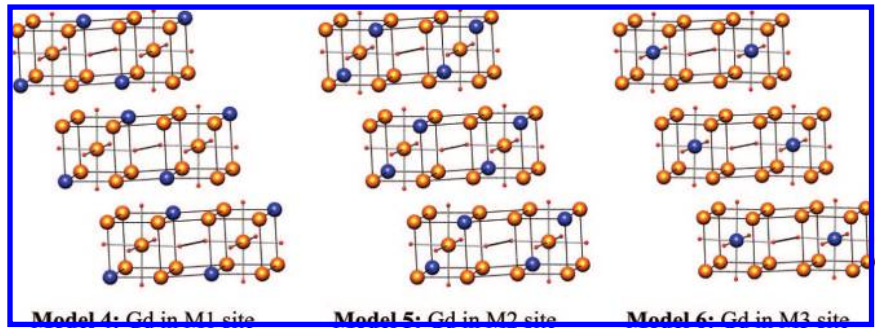

Figure 7. Three model structures of GdY_4Ge_4 studied by TB-LMTO-ASA and LSDA calculations. Blue spheres are Gd, orange spheres are Y, and smaller red spheres are Ge.

Table 6. Crystallographic Data for $Gd_{5-x}Y_xGe_4$ (x = 3.8, 4.0, and 4.2) As Obtained by Single Crystal X-ray Diffraction[a]

x	3.8	4.0	4.2
loaded composition	$Gd_{1.2}Y_{3.8}Ge_4$	GdY_4Ge_4	$Gd_{0.8}Y_{4.2}Ge_4$
refined composition	$Gd_{1.11(3)}Y_{3.89}Ge_4$	$Gd_{1.00(3)}Y_{4.00}Ge_4$	$Gd_{0.77(3)}Y_{4.23}Ge_4$
independent reflections	1014	1021	1010
No. of parameters	47	47	47
final R indices [$I > 2\sigma(I)$]	$R1$ = 0.0434, w$R2$ = 0.0826	$R1$ = 0.0426, w$R2$ = 0.0769	$R1$ = 0.0332, w$R2$ = 0.0574
peak/hole (e/Å^3)	1.979/−1.496	1.623/−1.439	1.408/−1.092

[a] Space group $P2_1/c$ (No. 14), Mo Kα radiation, 2θ range = 4−57°, T = 298(2) K, Z = 2.

Table 7. Atomic Coordinates, Site Occupancies, and Isotropic Displacement Parameters for $Gd_{5-x}Y_xGe_4$ (x = 3.8, 4.0, and 4.2) As Obtained by Single Crystal X-ray Diffraction[a]

atom		x	y	z	occupancy[b]	U_{eq}[c] (Å^2)
			$Gd_{1.11(3)}Y_{3.89}Ge_4$			
M1	4e	0.7006(1)	0.3217(1)	0.0574(1)	0.35(1)	0.010(1)
M2	4e	0.2659(1)	0.3371(1)	0.2775(1)	0.15(1)	0.009(1)
M3	2a	0	0	0	0.11(1)	0.009(1)
Ge1	4e	0.4115(2)	0.0314(2)	0.1807(2)	1	0.010(1)
Ge2	4e	0.0082(2)	0.6300(2)	0.1286(2)	1	0.010(1)
			$Gd_{1.00(3)}Y_{4.00}Ge_4$			
M1	4e	0.7007(1)	0.3219(1)	0.0571(1)	0.32(1)	0.011(1)
M2	4e	0.2658(1)	0.3373(1)	0.2776(1)	0.13(1)	0.009(1)
M3	2a	0	0	0	0.09(1)	0.009(1)
Ge1	4e	0.4112(2)	0.0312(1)	0.1807(2)	1	0.010(1)
Ge2	4e	0.0083(2)	0.6300(1)	0.1286(2)	1	0.011(1)
			$Gd_{0.77(3)}Y_{4.23}Ge_4$			
M1	4e	0.7008(1)	0.3219(1)	0.0569(1)	0.25(1)	0.010(1)
M2	4e	0.2656(1)	0.3371(1)	0.2779(1)	0.10(1)	0.009(1)
M3	2a	0	0	0	0.07(1)	0.008(1)
Ge1	4e	0.4112(1)	0.0314(1)	0.1809(1)	1	0.010(1)
Ge2	4e	0.0083(1)	0.6302(1)	0.1287(1)	1	0.010(1)

[a] Coordinates are represented in accordance with similar previously reported structure types. [b] All M1, M2, and M3 sites are fully occupied with a mixture of Gd and Y atoms. Only Gd occupations are listed. [c] U(eq) is defined as one-third of the trace of the orthogonalized U_{ij} tensor.

respectively. The effective magnetic moments for the series were determined to be 7.89(1)−7.47(1) μ_B/Gd ion (theoretical value for Gd^{3+} = 7.94 μ_B) based on numerical fits for the data between 150 and 270 K. The effective magnetic moments for the two Y-rich phases are lower than the expected value and the reason is not well understood. But because the results were reproducible, it could probably be attributed due to the presence of some unidentified noncrystalline minority phases.

Magnetic susceptibility measurements for the $Gd_{5-x}Y_xSi_4$ series were also carried out between 6 and 300 K. All phases undergo ferromagnetic ordering showing Curie−Weiss behavior at high temperatures. This transition for Gd_4YSi_4 exceeds 300 K, but for $Gd_3Y_2Si_4$ (T_C = 203(2) K), $Gd_2Y_3Si_4$ (T_C = 133(2) K), and GdY_4Si_4 (T_C = 50(2) K), the Curie temperatures decrease almost linearly with increasing Y concentration. These susceptibility plots are included in the Supporting Information.

Theoretical Electronic Structure. Substitution at the RE metal sites raises a number of questions. In this paper, we specifically focus on the problems for the Ge-system. For this, electronic structure calculations were carried out on two, near-end members of the $Gd_{5-x}Y_xGe_4$ series, Gd_4YGe_4 and GdY_4Ge_4, to gain an understanding as to how electronic forces affect the following three issues: (1) the distribution of Gd and Y among the three metal sites, which is known as the coloring problem;[38] (2) the structural transformation from orthorhombic to monoclinic crystal class; and (3) the magnetic ordering behavior.

(38) Miller, G. J. *Eur. J. Inorg. Chem.* **1998**, *5*, 523.

Table 8. Summary of Relative Total Energies and Magnetic Moments per Gd Atom Calculated for the Models of Gd_4YGe_4 and GdY_4Ge_4 by TB-LMTO-ASA and LSDA

model	minority atom site	LDA (meV)	LSDA (meV)	moment/Gd (BM)
		Gd_4YGe_4		
1	M1	+268	+267	7.27
2	M2	+281	+275	7.29
3	M3	0	0	7.27
		GdY_4Ge_4		
4	M1	0	0	7.38
5	M2	+127	+138	7.29
6	M3	+355	+355	7.52

Coloring Problem. For all $Gd_{5-x}Y_xTt_4$ systems where Tt = Si, Ge, the M sites are all fractionally occupied by Gd and Y atoms: the M3 sites are Y-rich and the M1 sites are Gd-rich. To probe the distribution of Gd and Y atoms among the M sites, we examined three model structures based on the experimentally determined orthorhombic Gd_4YGe_4 and monoclinic GdY_4Ge_4: Model **1** (**4**) contains Y (Gd) in 50% of M1 sites and Gd (Y) in M2 and M3 sites; Model **2** (**5**) contains Y (Gd) in 50% of M2 sites and Gd (Y) in M1 and M3 sites; Model **3** (**6**) contains Y (Gd) in M3 site and Gd (Y) in M1 and M2 sites. These model structures are illustrated in Figures 6 and 7; the coloring schemes of Gd and Y atoms were selected to maintain either the mirror plane or inversion center, respectively, within the slabs building up Gd_4YGe_4 and GdY_4Ge_4. According to the total energies per formula unit, which are listed in Table 8, Models **3** and **4**, respectively, are the preferred arrangements of Gd and Y atoms for Gd_4YGe_4 and GdY_4Ge_4. Both energetic conclusions indicate that it is most favorable for the Y atoms to occupy the M3 sites and Gd atoms to occupy the M1 sites. This fact is consistent with the refined site occupancies obtained from single crystal diffraction results (see Figure 4), as well as from size arguments as based upon the local coordination environments for the different M sites. The M3 site shows the shortest M−M contacts and has the smallest volume of the different M sites in these structures. Nevertheless, the calculated total energies also suggest an influence from the local electronic structure toward influencing the observed coloring.

An alternative way to study the coloring problem in this series by electronic structure calculations is to compare the valence electron numbers assigned to each M site for the binary examples, Gd_5Ge_4 and Y_5Ge_4, both of which crystallize in the orthorhombic structure at room temperature. For semiempirical methods, valence electron numbers correspond to Mulliken populations, for example; in TB-LMTO-ASA, we can approximate these numbers for each atomic site by the sum of integrated electron densities within each WS sphere for the atoms, which are called QVAL values. An alternative approach is to integrate the occupied density of states for each site, which we call IDOS. As a qualitative interpretation, QVAL values are determined from real-space electron densities; IDOS values from reciprocal-space electron densities. The sum of either QVAL or IDOS values will equal the total number of valence electrons in the chemical formula. The TB-LMTO-ASA results for Gd_5Ge_4 and Y_5Ge_4 are listed in Table 9. In both cases, the greatest build up of valence electrons at the M sites, as indicated by the highest QVAL value, occurs at the M3 site (center) and the fewest at the M1 and M2 sites (edges). From the diffraction and coloring problem results, Y prefers to occupy the M3 sites and Gd prefers to occupy the M1 sites. According to this alternative perspective for ternary $Gd_{5-x}Y_xGe_4$ phases, Y also prefers the site which has a highest density of valence electrons, whereas Gd prefers the site(s) that has a lower density of valence electrons.

Table 9. QVAL and IDOS Values Evaluated for Each Site in the Asymmetric Units for Gd_5Ge_4 and Y_5Ge_4[a]

	Gd_5Ge_4[V = 222.4 Å^3]		Y_5Ge_4[V = 215.8 Å^3]	
	QVAL	IDOS	QVAL	IDOS
M1 (edge)	2.916	2.899	2.844	2.843
M2 (edge)	2.916	2.899	2.844	2.843
M3 (center)	3.355	3.322	3.333	3.334
Ge1 (BeS)	4.167	4.157	4.283	4.280
Ge2 (WiS)	3.824	3.816	3.863	3.861
Ge3 (WiS)	3.824	3.815	3.863	3.861

[a] The location of the sites is indicated in parentheses: edge = edge of slabs; center = center of slabs; BeS = between slabs; WiS = within slabs. V' = volume per formula unit.

These results corroborate well with the trends in the sequence of ionization energies to form M^{3+} ions from the gaseous atoms. The first three ionization energies for Gd are, respectively, 595, 1172, and 1999 kJ/mol, whereas those for Y are 616, 1181, and 1980 kJ/mol.[39] In chemically reduced environments for Gd and Y when both elements occur simultaneously, as observed for $Gd_{5-x}Y_xGe_4$, Gd atoms will tend to lose valence electrons more readily than Y atoms. Thus, in such structures, Gd atoms will occupy sites with lower valence electron concentrations than Y atoms. However, the results listed in Table 9 for Gd_5Ge_4 and Y_5Ge_4 cannot be directly compared as the QVAL or IDOS values were calculated for different unit cell volumes, atomic positions, and basis functions for the atomic orbitals.

An additional observation from Table 9 is that the Ge sites separate clearly into two chemically distinct environments, which is in accord with earlier electronic structure calculations.[21] The Ge1 sites attract greater electron density than the Ge2 and Ge3 sites within the slabs. The long Ge1−Ge1 distance between slabs but the shorter Ge2−Ge3 contact within slabs have rationalized the Zintl-type formalism $(Gd^{3+})_5(Ge_2)^{6-}(Ge^{4-})_2$: in Table 9, the Ge1 sites correspond to the more reduced Ge sites (Ge^{4-}) and the Ge2 and Ge3 sites are less reduced and share a valence electron pair (Ge_2^{6-}).

Structural Transformation Problem. To elucidate possible electronic factors that might influence the structural variation in the $Gd_{5-x}Y_xGe_4$ series, idealized model structures of monoclinic GdY_4Ge_4 and orthorhombic Gd_4YGe_4 were constructed from topologically identical slabs. An idealized, isolated slab would have tetragonal symmetry with the 4-fold rotation axes intersecting the M3 sites at the centers of every cube of M sites. However, this rotational symmetry is destroyed when the slabs form the various structures in $Gd_{5-x}Y_xGe_4$. In the monoclinic GdY_4Ge_4 structure, space group $P2_1/c$, there is one slab per unit cell with the M3 site coincident with an inversion center; in the orthorhombic Gd_4YGe_4 structure, space group *Pnma*, there are two slabs per unit cell and each slab contains a mirror plane through the middle of each slab intersecting the M3, Ge2, and Ge3 sites. Therefore, to take into account these features as well as the results of the coloring problem for Gd and Y atom, our models have the following common features: (i) the two lattice constants identifying the periodicity within each slab are set equal, that is, $b_M = c_M$ in the monoclinic case with $\beta = 113.042°$ and $a_O = c_O$ in the orthorhombic case;[40] (ii) the lattice metrics

(39) Greenwood, N. N.; Earnshaw, A. Chemistry of the Elements; Elsevier Butterworth-Heinemann: Oxford, 1997.

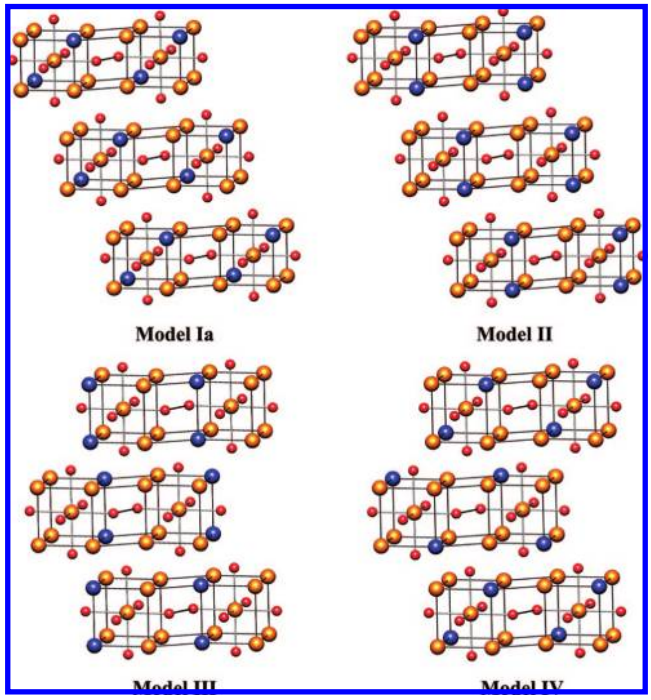

Figure 8. Structural models of GdY_4Ge_4. Blue spheres are Gd, orange spheres are Y, and red spheres are Ge sites.

and site positions are selected to mimic as closely as possible the nearest neighbor distances in the observed structures; (iii) the 3^2434 nets formed by the M1 and M2 sites in each slab are strictly planar; and (iv) the distribution of Gd and Y atoms are in accord with the results of the coloring problem. For these calculations, the WS radii for each atomic site in the asymmetric units were kept the same in the different models, which encompassed both monoclinic and orthorhombic crystal classes for the two compositions.

GdY_4Ge_4. Figure 8 illustrates the four structural models studied. The lattice parameters for the different crystal classes were also restricted as follows: $a_O = c_O = b_M = c_M$ and $a_O \cdot b_O \cdot c_O = 2(a_M \cdot \sin\beta) \cdot b_M \cdot c_M$, where a_O, b_O, c_O are the lattice parameters for a hypothetical orthorhombic structure; a_M, b_M, c_M, and β are the lattice parameters for the monoclinic structure of GdY_4Ge_4 obtained from PXRD. As evident from Figure 8, to obtain the formula GdY_4Ge_4, each 3^2434 metal layer contains 25% Gd atoms. Furthermore, the Gd distribution in models **Ia** and **IV** locate inversion centers at the M3 sites (this inversion center in **IV** is strictly lost in the complete 3D structure);[41] for models **II** and **III**, each slab shows local mirror symmetry containing the M3 sites (again, this mirror plane in **II** is lost in the complete 3D structure). The total energies listed in Table 10 show that model **Ia**, which has a monoclinic structure with its inversion center intact, is the most favorable configuration, which matches our experimental results very well; in fact, the two monoclinic models give the lowest energies.

Gd_4YGe_4. Following to the results of the coloring problem, Y was placed at the M3 site, which is the center of the pseudocubes of Gd atoms. The orthorhombic model (**V**) is model **3**, as shown in Figure 6; the monoclinic model (**VI**) is model **6** (see Figure 7), but with orange spheres representing Gd and blue spheres representing Y. The lattice parameters for the two structures also followed the restrictions: $a_O = c_O = b_M = c_M$ and $(a_M \cdot \sin\beta) \cdot b_M \cdot c_M = {}^1/_2 a_O \cdot b_O \cdot c_O$, where a_M, b_M, c_M, and β are the lattice parameters for the hypothetical monoclinic structure; a_O, b_O, and c_O are the lattice parameters for the orthorhombic structure of Gd_4YGe_4 obtained from PXRD. The total energies listed in Table 11 show that model **V** is energetically more favorable, which also matches well with our experimental results.

These preliminary theoretical results suggest the interplay among the site preferences for Gd and Y, the local symmetry features of an individual slab, and the local electronic structures of Gd and Y atoms. In GdY_4Ge_4, the minority Gd atoms seek the M1 or M2 sites. These sites accumulate the lowest electron density, so we infer that electrostatic factors maximize the separation between adjacent Gd atoms, and this creates the inversion center for an isolated slab. The valence electron numbers (QVAL values) listed in Table 10 confirms this charge distribution: Y sites are electron rich, whereas Gd sites are electron poor. The stacking mode thus follows monoclinic symmetry. For Gd_4YGe_4, the majority Gd atoms also seek the M1 and M2 sites; Y prefers the M3 sites at the interior of the slabs. Again, the Gd sites are electron poor;

Table 10. Relative Total Energies, Average QVAL, and IDOS Values for Each of the Metal and Ge-Sites in the Model Structures for GdY_4Ge_4[a]

	monoclinic (model **Ia**) E/f.u. = 0 meV		monoclinic (model **II**) E/f.u. = +133.33 meV	
	QVAL	IDOS	QVAL	IDOS
M1 (edge)	3.278	3.263	3.277	3.262
M2 (edge)	2.599	2.585	2.606	2.592
M3 (center)	3.750	3.730	3.749	3.730
Ge1 (BeS)	3.975	3.968	3.973	3.966
Ge2 (WiS)	3.772	3.765	3.770	3.763
	orthorhombic (model **III**) E/f.u. = +160.82 meV		orthorhombic (model **IV**) E/f.u. = +361.58 meV	
	QVAL	IDOS	QVAL	IDOS
M1 (edge)	3.312	3.300	3.311	3.295
M2 (edge)	2.576	2.567	2.583	2.570
M3 (center)	3.747	3.733	3.749	3.727
Ge1 (BeS)	3.967	3.963	3.962	3.956
Ge2/Ge3 (WiS)	3.772	3.766	3.769	3.761

[a] The location of the sites is indicated in parentheses: edge = edge of slabs; center = center of slabs; BeS = between slabs; WiS = within slabs. (f.u. = formula unit).

Table 11. Relative Total Energies, Average QVAL and IDOS Values for Each of the Metal and Ge Sites in the Model Structures for Gd_4YGe_4[a]

	orthorhombic (model **V**) E/f.u. = 0 meV		monoclinic (model **VI**) E/f.u. = +331.72 meV	
	QVAL	IDOS	QVAL	IDOS
M1 (edge)	2.910	2.898	2.878	2.871
M2 (edge)	2.910	2.897	2.983	2.976
M3 (center)	3.364	3.341	3.360	3.349
Ge1 (BeS)	4.172	4.163	4.140	4.135
Ge2/Ge3 (WiS)	3.826	3.819	3.818	3.815

[a] The location of the sites is indicated in parentheses: edge = edge of slabs; center = center of slabs; BeS = between slabs; WiS = within slabs. (f.u. = formula unit).

(40) The coordinates and the lattice parameters used for building both orthorhombic and monoclinic structural models are provided in Supporting Information.

(41) A different coloring of Gd atom in the monoclinic structure was also studied as model **Ib**. The calculation results and the structural figure are included in Supporting Information.

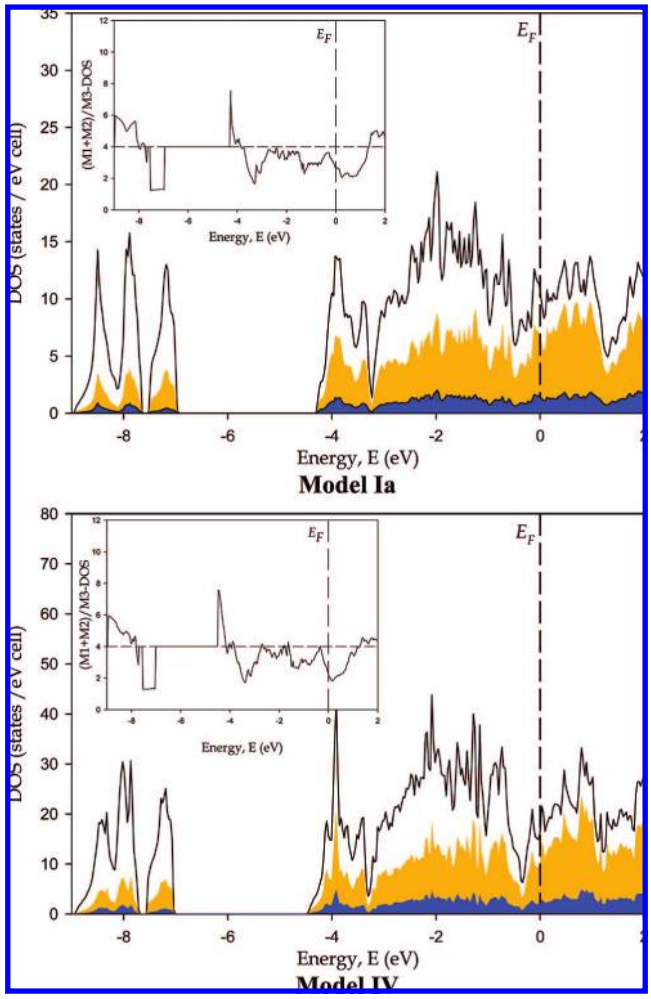

Figure 9. DOS plots for GdY_4Ge_4. Total DOS (white region), Y PDOS (orange region), and Gd PDOS (blue region). The insets show the variation of (M1 + M2)/M3 − DOS with energy.

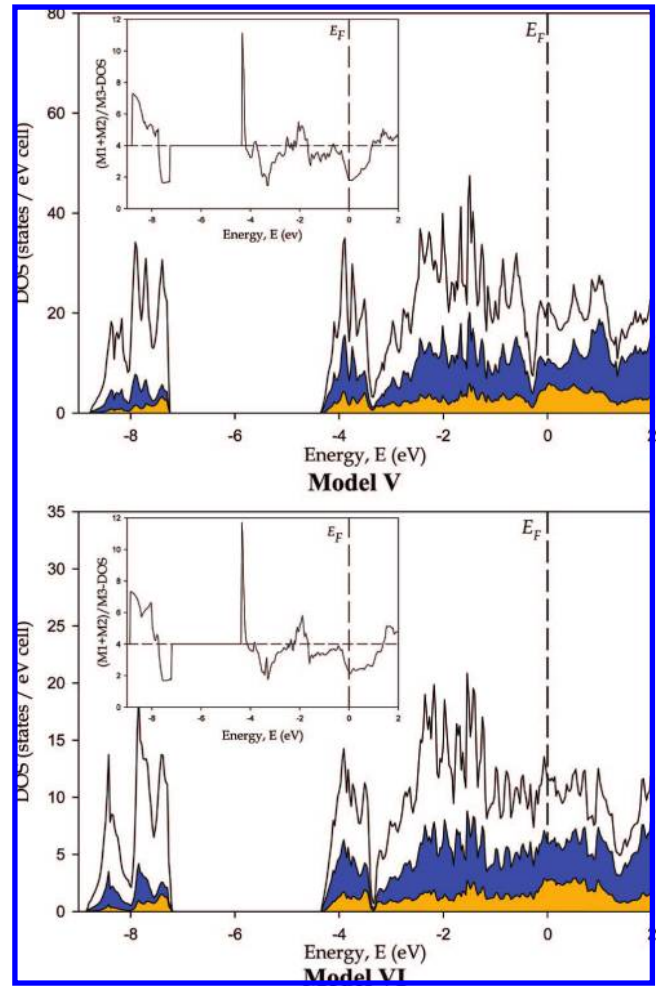

Figure 10. DOS plots for Gd_4YGe_4. Total DOS (white region), Gd PDOS (blue region), and Y PDOS (orange region). The insets show the variation of (M1 + M2)/M3 − DOS with energy.

the Y sites are electron rich. In this structural configuration, each slab has both mirror and inversion symmetry. In this case, the mirror plane is retained while the inversion center is lost for the orthorhombic stacking pattern (**V**). In this situation, further theoretical assessment is required.

The DOS plots for two models each of GdY_4Ge_4 and Gd_4YGe_4 are shown, respectively, in Figures 9 and 10. Common features to all four curves include (i) three peaks between −9.0 and −7.0 eV, with the two end peaks representing the bonding σ_s and antibonding σ_s* states of the short Ge_2 dimers and the middle peak being the nonbonding state of the interslab Ge monomers, all with contributions from Gd and Y orbitals; (ii) states between −4.5 eV to just below the Fermi level, involving significant combinations of Ge 4*p*, Y 5*s*, and 4*d*, and Gd 6*s* and 5*d* orbitals; and (iii) states just above the Fermi level, which are largely Y 5*s* and 4*d* and Gd 6*s* and 5*d* orbitals. Also, all of them show two pseudogaps in the region between −4.5 eV to just below the Fermi level: these states are derived from the 4*p* bonding states and 4*p* lone pairs of Ge_2 dimers that interact in a bonding manner with the metal *s* and *d* orbitals, which are also involved in M−M bonding. From integration of the DOS curves, the electron count at the lower energy pseudogap is about 12 electrons per formula unit for both GdY_4Ge_4 and Gd_4YGe_4; the pseudogap closer to the Fermi level ranges from about 29−30 valence electrons per formula unit. Because the interslab Ge−Ge contacts exceed about 3.6 Å, we can treat each Ge atom as isoelectronic with noble gas atoms and would, therefore, carry a formal charge of −4. The intraslab Ge_2 dimers can be treated to be isoelectronic with halogen dimers and, hence, would carry a formal charge of −6. Hence, we can write the chemical formula of $(Gd/Y)_5Ge_4$ as $(Gd^{3+}/Y^{3+})_5(Ge_2^{6-})(Ge^{4-})_2(1e^-)$. This formalism accounts for 30 valence electrons per formula unit needed to occupy states up to the second pseudogap, just below the Fermi level. Now, as $(Gd/Y)_5Ge_4$ has 31 valence electrons per formula unit, the additional electron will occupy the narrow band just above this second pseudogap.

The insets in all the DOS plots show the contributions of the M1 and M2 sites to the total DOS with respect to that from the M3 sites, that is, (M1 + M2)/M3. Now, because the ratio of the number of metal sites at the edges (M1/M2) to the number of metal sites at the center (M3) in both orthorhombic and monoclinic structures is 4:1, these curves have a baseline at $y = 4$, which is indicated by the dashed horizontal line. The interesting feature that stands out from these plots is that the contribution to the DOS from the M3 sites near the Fermi level is about twice that from (M1 + M2) sites, in spite of the 4:1 ratio. Moreover, LSDA + U

Table 12. Summary of Relative Total Energies and Local Magnetic Moments Calculated for Two Different Models of GdY_4Ge_4 and Gd_4YGe_4 by TB-LMTO-ASA

	GdY_4Ge_4		Gd_4YGe_4	
	monoclinic (model **Ia**): E_{NM} = 8690 meV		*orthorhombic* (model **V**): E_{NM} = 34760 meV	
	Ferromagnetic	Antiferromagnetic	Ferromagnetic	Antiferromagnetic
E (meV)	0.000	7.68	11.98	0
μ (M1)	Gd: 7.243	Gd: ±7.242	Gd: 7.228	Gd: ±7.245
μ (M2)	Y: 0.009	Y: ±0.002	Gd: 7.228	Gd: ±7.244
μ (M3)	Y: 0.043	Y: ±0.043	Y: 0.133	Y: ±0.146
μ (Ge1)	−0.003	∓0.002	−0.028	∓0.019
μ (Ge2)	−0.003	∓0.003	−0.029	∓0.028
μ (Ge3)			−0.029	∓0.028

calculations[26,42] show that the magnetic moment for the M3 site is greater than that for either the M1 or M2 site. Hence, we can conclude that the M3 site acts decisively in shaping the magnetic and structural features observed in these RE_5T_4 systems.

Magnetic Ordering Problem. The results of LSDA calculations for the lowest energy models of GdY_4Ge_4 (model **Ia**) and Gd_4YGe_4 (model **V**) are presented in Table 12. In both cases, magnetically ordered patterns achieve lower total energies self-consistently than the corresponding nonmagnetic cases. This approach successfully agrees with our experimental results: GdY_4Ge_4 prefers ferromagnetic ordering; Gd_4YGe_4 prefers antiferromagnetic ordering. The lowest energy magnetic ordering patterns show completely ferromagnetic coupling within the structural slabs that serve as the building blocks for the entire $Gd_{5-x}Y_xGe_4$ series. Orthorhombic Gd_4YGe_4, therefore, exhibits antiferromagnetic coupling between adjacent slabs; ferromagnetic coupling within slabs for a net zero magnetization.

Table 12 also summarizes the local magnetic moments obtained by each calculation. Local moments at the Ge sites are negligibly small and there is a slight polarization occurring at the Y sites. For all models, Y atoms at the M3 sites (center of the pseudocubes within each slab) show the greater local moments than for Y atoms located at the M1 or M2 sites. Because the DOS curves in Figures 9 and 10 emphasize the significance of valence *s* and *d* orbitals of the M3 sites at the Fermi levels in this series, their magnetic behavior is strongly influenced by exchange coupling between the M3 sites and the M1 or M2 sites of the slabs. With just a single effective conduction electron in $Gd_{5-x}Y_xGe_4$, ferromagnetic coupling within the slab is anticipated by this low band filling.[43] Further calculations, however, are required to elucidate the factors contributing to the magnetic exchange between slabs. Nevertheless, other substitution patterns in various $Gd_{5-x}RE_xGe_4$ examples (RE = La, Lu, Sc)[26,35] also show interesting variations in magnetic behavior.

Conclusions

A crystal chemical analysis of the distribution of Gd and Y atoms over the various metal sites in the $Gd_{5-x}Y_xTt_4$ (*Tt* = Si, Ge) series has been presented. All silicides adopt the orthorhombic Gd_5Si_4-type structure with short Si−Si contacts between the slabs, which form the primary structural building blocks for these structures. All germanides exhibit long Ge−Ge contacts between these slabs at room temperature, but do show a change in stacking pattern near GdY_4Ge_4 to a monoclinic, $U_2Mo_3Si_4$-type structure. Single crystal diffraction results reveal a preference of the smaller Y atoms to occupy the M3 sites (centers of slabs), whereas the larger Gd atoms prefer to occupy the M1 sites (edges of slabs). Furthermore, the calculated electronic structures for $Gd_{5-x}Y_xGe_4$ show that this preference can also be attributed to the density of valence electrons at the various M-sites: Y prefers the site with the highest density of valence electrons (M3), whereas Gd prefers the site(s) with a lower density of valence electrons (M1/M2). It is this interaction among the site preferences and electronic factors that drives the structural transformation from orthorhombic, Sm_5Ge_4-type to a previously unreported monoclinic, $U_2Mo_3Si_4$-type structure in the $Gd_{5-x}Y_xGe_4$ series. The calculation results also illustrate the central importance of the M3 site in molding the magnetic properties and the structural features observed for these RE_5T_4 systems. It is, therefore, further emphasized and confirmed that these nanometer-sized slabs, centered by the M3 site, can truly be regarded as the fundamental building blocks for many of the structures observed within these systems.

The differences, however, between $Gd_{5-x}Y_xGe_4$ and $Gd_{5-x}Y_xSi_4$ remain to be understood, as the silicides phases retain the robust O(I) structure for compositions with $x < 5$ (Y_5Si_4 adopts the monoclinic $Gd_5Si_2Ge_2$ structure[44]), whereas the germanides phases exhibit the monoclinic $U_2Mo_3Si_4$-type structure for values of x close to 4.0. Although one can speculate about chemical pressure imposed by replacing Ge atoms with the smaller Si atoms, changes in specific RE−RE, RE−*Tt*, and *Tt*−*Tt* interactions have not been evaluated. Investigations of mixed metal and mixed tetrelide systems, that is, $Gd_{5-x}Y_x(Si, Ge)_4$, as well as an additional theoretical study of the site preferences and electronic structures of $Gd_{5-x}Y_xSi_4$ are underway.

Acknowledgment. The authors thank Prof. Vitalij Pecharsky and Mr. Roger Rink for using the Lakeshore Magnetometer. This work was carried out at the Ames Laboratory, which is operated for the U.S. Department of Energy by Iowa State University under Contract No. DE-AC02-07CH11358. This work was supported by the Materials Sciences Division of the Office of Basic Energy Sciences of the U.S. Department of Energy.

Supporting Information Available: X-ray crystallographic data in CIF format, for $Gd_{5-x}Y_xSi_4$ ($0 \le x \le 4$) and $Gd_{5-x}Y_xGe_4$ ($0 \le x \le 5$) series, lattice parameters, and coordinates for the various models studied, magnetic susceptibility plots for the $Gd_{5-x}Y_xSi_4$ series, and $M(H)$ plots for the $Gd_{5-x}Y_xGe_4$ series. This material is available free of charge via the Internet at http://pubs.acs.org.

JA802848R

(42) Paudayl, D.; Pecharsky, V. K.; Gschneidner, K. A., Jr.; Harmon, B. N. *Phys. Rev. B* **2007**, *75*, 094427.

(43) (a) Samolyuk, G.; Fokwa, B. P. T.; Dronskowski, R.; Miller, G. J. *Phys. Rev. B* **2007**, *76*, 094404. (b) Samolyuk, G.; Miller, G. J. *J. Comput. Chem.* **2008**, *29*, 2177.

(44) Pecharsky, A. O.; Pecharsky, V. K.; Gschneidner, K. A., Jr. *J. Alloys Compd.* **2004**, *379*, 127.